Multi-Objective Optimisation of Heat Transfer Elements within A Rotary Regenerative Heater

Jordan White, Marco Vezza
University of Glasgow
University Avenue, Glasgow, G12 8QQ
j.white.3@research.gla.ac.uk
Marco.Vezza@glasgow.ac.uk

Abstract

In the current climate change crisis, power generation and other large emission industries are under pressure to improve efficiency and cut emissions. Rotary regenerative heaters provide a way to recycle heat from exhaust gas, greatly improving efficiency in boiler heating, emissions treatment, and other areas. Modifying the shape of storage plates within the rotary heater can augment heat transfer whilst retaining flow pressure, allowing for more efficient heat recycling. This study uses Computational Fluid Dynamics (CFD) to perform multi-objective optimisation on a common style of element plate. Pitch and radius of the Flat-Notched-Crossed style element plate were varied to measure the effect on heat transfer and pressure drop characteristics. It was found that both variables significantly affected the performance of the element. Further analysis showed that vortex generation and turbulent mixing were the main source of increased heat transfer and strategically controlling the vortical flow structure improved pressure retention through the part. While there is a general consensus that a larger surface area facilitates increased heat transfer, this study concludes that vorticity and turbulence control are significant factors to the performance of the element design.

Keywords – heat transfer, rotary heater, optimisation, CFD

1. Introduction

Due to pressure from climate change treaties and deadlines, it is becoming increasingly important to reduce emissions and improve efficiency in all areas. Rotary regenerative heaters are a versatile solution to enhance efficiency and facilitate emissions reduction through recycling waste heat. The technology stores heat from exhaust gas in a dense matrix of steel elements before rotating out of the exhaust and into the inlet where the heat is transferred to the inlet flow. This process effectively transfers heat from the exhaust to the intake without mixing the gas flows. Rotary regenerative heaters benefit from reduced size and cost when compared to plate or shell-and-tube heat exchangers for larger scale applications. [1]

This paper will focus on the elements in the heat storage matrix. Since the first rotating-plate air preheater (RAPH) was created by Ljungstrom in 1920, [2], the element plate designs have changed significantly. By altering the shape of these plates, increased heat transfer rates can be achieved. Element design has become so integral to the performance of the heater, most new research is shrouded in industrial secrecy. Whilst there is no doubt that new cutting-edge element designs are present in rotary heaters around the world, the general state of published research is lacking. The most common element designs test in research are flat-notched-crossed, double undulated (DU) and corrugated-undulated (CU). The Flat Notched Crossed design is generally the best performing element out of the three. These element designs are available in the public domain as they are outdated and generally obsolete, [3]. However, the wide availability of these styles of element facilitates a rich seam for research as there is still a great deal to learn about the flow characteristics and performance in rotary heaters.

This study aims to use CFD methods to optimise the Flat Notched Crossed style element plate by varying the geometric dimensions of the design. Through this optimisation, a CFD comparison of the flow characteristics can be made between the optimal and base design to develop an understanding of the factors affecting the heat transfer and pressure retention performance of the heat transfer elements.

Research progress in the element design area is generally slow due to the difficulty in accurately modelling the flow through the element passages. Studies have shown that complex flow patterns, including secondary swirling flows are prevalent due to the abundant crossflows stemming from the typical crossed/corrugated designs with the purpose of

inducing turbulent mixing, [4] [5]. These flow patterns, combined with the small-scale complex geometry over large element plates, create significant difficulties in accurately capturing the flow behaviour in CFD simulations as enormous computational power is required in order to study such intricate and detailed scenarios. Several studies have attempted to create efficient CFD simulations of RAPH elements, using techniques such as periodic boundaries and steady flow average turbulence solvers. [6]

Other research has found success in physical experiments. Stasiek used a test rig to measure the effect of the corrugation angle, plate pair height, pitch and Reynolds number on pressure drop and heat transfer performance. It was found that increasing the angle improved the heat transfer performance, but also increased the friction factor. Similar results were seen for the other variables. This study used liquid crystals to measure the flow characteristics. The research concludes that altering the angle makes the largest change as it fundamentally alters the flow structure through the heat exchanger. [7]

2. Experimental Methods

This study will use STAR-CCM+ CFD methods to simulate the flow through rotary heater elements. The simulation will closely resemble, and be validated by, a rotary heater element test rig in Glasgow, UK. The study will then use the validated model to optimise the pitch and radius dimensions of the Flat Notched Crossed plate and analyse the results.

2.1 Experimental Test-Rig

The test rig consists of an element chamber capable of containing around 12 element plates depending on the height of each plate. It tests a small section of an element basket (900mm long, 300mm wide, 150mm high) for pressure drop and heat transfer. Heated air is pumped through the element basket with various pressure and temperature sensors measuring the flow data across the element basket. The rig measures the pressure drop and heat transfer across a Reynolds number range of 1000-3500. The temperature of the air oscillates between 303K and 323K in a sinusoidal pattern over a period of 25.71 seconds to emulate the heating and cooling cycle of a RAPH. This allows for heat transfer and pressure drop data to be gathered in order to evaluate the element profile. This data is gathered via an array of sensors at the inlet and outlet of the element chamber.

2.2 CFD Simulation Model

A model was created in Solidworks of the Flat Notched Crossed plate used in the experimental test rig (Figure 1). A solid and fluid part are created separately and are assigned to solid and fluid regions in STAR-CCM+.
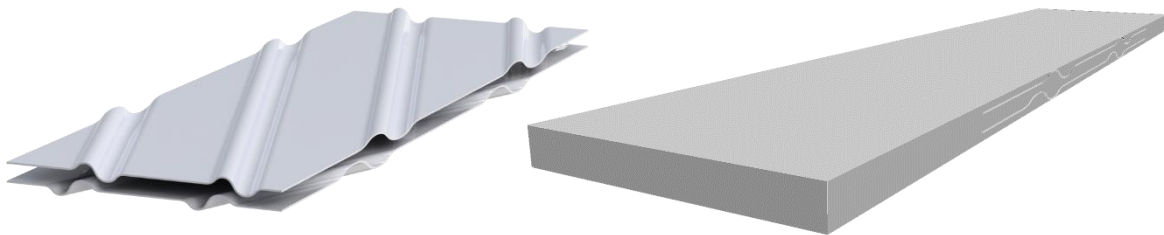

Figure 1. Flat Notched Crossed model parts

The CFD simulation is designed to replicate the element basket in the test rig. Inlet conditions are added for the sinusoidal temperature oscillation and the flow velocity. The flow velocity is varied through Reynolds numbers 1500-3500, to correlate with the test rig. It should be noted that studies have shown that transitional flow is encountered in narrow passages for Reynolds number 1500-3500 [5].

Simulating the airflow through an air preheater can be extremely difficult due to the large and complex structure. The complexity requires a very fine mesh structure, requiring enormous amounts of computational power to fully model,

making it unfeasible and inefficient for research purposes. It is therefore necessary to simplify the model where possible and prioritize the model to focus on a specific aspect. Similar studies have shown it is possible to accurately model the behaviour through the element pack while using periodic boundaries to simulate a full pack of elements whilst modelling a small amount with cut down widths. This technique is very popular in turbomachinery research, where a single turbine blade channel is modelled and periodic boundaries are used to simulate a full blade ring. [8]

As the whole pack is made up of identical element pairs, one pair of elements should provide enough information to correctly model the flow conditions and generate accurate results. Additionally, to further conserve computational power, only a small section of the model is used. As the profile is a repeated pattern over the element plate, it can be useful to model a small part of the element plate and use periodic boundaries to replicate the rest of the plate. This allows a further reduction in cell count, allowing for faster and more efficient simulations to be run. Therefore, periodic boundaries are used on the top and bottom surfaces of the fluid region so that only 2 element plates are required, and the width is reduced by a factor of 4 with left-and-right-side periodic boundaries.

The STAR-CCM+ simulation is set up as a turbulent implicit unsteady flow regime, with the use of the segregated flow solver and the WALE Large Eddy Simulation (LES) solver. The appropriate selection of physics models is imperative to a successful simulation. While various physics models may result in similar numerical results, it is important to understand the pros and cons of each model in regards to the priorities of the investigation. RANS is more computationally efficient, but only provides the mean flow characteristics. Therefore, it is useful for calculating pressure drop/heat transfer, however, will not show the detailed turbulent flows within the part model, [9]. LES provides good technical information about the turbulence within a flow, at the cost of an increased computational power requirement. Studies have shown that LES provides greater accuracy in both quantitative measurements and qualitative data when compared with RANS. Results more accurately follow experimental data, and the turbulence has a closer visual resemblance to experimental data. [10]

The temperature oscillation is implemented with Equation 1, with 5 seconds added to allow the simulation to settle from its initial transient response.

$$T_{inlet} = 313 + 10\sin\bigl(0.2443467934(t-5)\bigr) \tag{1}$$

2.2 Mesh grid

A mesh grid independence analysis was performed to find the optimal mesh grid to balance accuracy with required computational power. The variables were set as base cell size and number of prism layers. The Reynolds number was set at 3200 as this point has the lowest calculated error in the experimental test rig results. The results are shown in Table 1 showing that the 3.5mm base size mesh grid with 8 prism layers provided the closest match to the experimental data.

Table 1. Mesh grid sensitivity analysis

Designation	Base size	Target surface size	No. prism layers	Number of cells (fluid)	Friction Factor	Colburn factor
FNoC_Test	-	-	-	-	0.1083	0.0079
FNoCM1	0.005	100	6	6,170,537	0.9983	0.00651
FNoCM2	0.004	100	6	7,467,104	0.1010	0.00689
FNoCM3	0.003	100	6	8,611,254	0.1042	0.00725
FNoCM4	0.0035	100	6	8,129,864	0.1076	0.00730
FNoCM5	0.002	100	6	9,718,386	0.1082	0.00731
FNoCM6	0.0035	100	8	8,593,298	0.1083	0.00786
FNoCM7	0.0035	100	10	9,909,254	No Convergence	

2.3 Measuring Data

The element profiles are analysed through the pressure drop and heat transfer performance. In the experimental data, these characteristics are measured through friction factor for pressure drop, and heat transfer coefficient and Colburn number for heat transfer.

2.3.1 Heat Transfer Coefficient

There are a few methods to calculate the heat transfer coefficient. The method used in the experimental test rig uses the difference between the inlet and outlet temperature, along with measurements of surface area, density, and other flow parameters.

In STAR-CCM+, a simpler method is available. STAR-CCM+ has a built-in heat transfer coefficient function, which measures the heat transfer coefficient on user-specified heat transfer surfaces. An average is taken from these boundaries, resulting in the mean heat transfer coefficient for the full model. This is calculated using Equation 2, a variation of Newton's law of cooling [11], [12].

$$h = \frac{q_{con}}{T - T_{ref}}$$
(2)

Where h is heat transfer coefficient, $(W/m^2 \cdot K)$, q_{con} is the conduction heat flux at the boundary, (W/m^2), T is boundary temperature (K), T_{ref} is reference temperature, (K).

The heat transfer performance is also measured with the Colburn factor. This is a widely used dimensionless factor which relates the Nusselt number, Reynolds number and Prandtl number. The Nusselt number is defined as the ratio of convective to conductive heat transfer across a boundary in a fluid. It is defined by Equation 3, [11], [13].

$$Nu = \frac{hD_h}{k}$$
(3)

Where Nu is Nusselt number, h is heat transfer coefficient, $(W/m^2 \cdot K)$, D_h is hydraulic diameter, (m), k is thermal conductivity, $(W/m \cdot K)$. Hydraulic diameter is calculated using Equation 4, [11].

$$D_h = \frac{4A}{P}$$
(4)

Where A is Area (m), P is Perimeter (m), which are measured in Solidworks using the measure tool. The Reynolds number is defined as the ratio of inertial forces to viscous forces within a fluid. It is defined by Equation 5, [11].

$$Re = \frac{\rho u L}{\mu}$$
(5)

Where Re is Reynolds number, ρ is density, (kg/m^2), u is velocity, (m/s), L is length, (m), μ is dynamic viscosity, $(Pa \cdot s)$. The Prandtl number is the ratio of momentum diffusivity to thermal diffusivity. It is defined in Equation 6 [11].

$$\text{Pr} = \frac{\mu . C_p}{k}$$
(6)

Where Pr is Prandtl number, μ is dynamic viscosity, $(Pa \cdot s)$, C_p is specific heat, $(J/kg \cdot K)$, and k is thermal conductivity, $(W/m \cdot K)$. Finally, the Colburn factor, J, relates heat transfer coefficients, mass transfer coefficients and friction factors. It is defined by Equation 7 [11].

$$J = \frac{Nu}{Re \cdot Pr^{\frac{1}{3}}}$$
(7)

2.3.2 Pressure Drop

The pressure drop characteristics are measured through "friction factor". This is a dimensionless scalable factor, allowing for easy comparison between test results. The friction factor is defined by the Darcy-Weisbach Equation, Equation 8 [14].

$$f = \frac{2 \cdot \Delta P \cdot D_h}{L \cdot \rho_{air} \cdot u^2}$$
(8)

Where:

f is friction factor, ΔP is pressure drop (Pa), D_h is hydraulic diameter (m), L is characteristic length (m), ρ_{air} is density of air (kg/m^2), u is inlet flow velocity (m/s).

The pressure drop is measured by recording the difference between the area-averaged pressure at the inlet and outlet throughout the simulation and taking a time-average.

The characteristic length is the distance from the inlet to the outlet of the element pack. The air density is found by taking a volume average for the full air region in STAR-CCM+. The inlet flow velocity is specified by the user but is also measured using an area average reading at the inlet in STAR-CCM+.

2.4 Optimisation

Optimisation can be a very useful tool when combined with CFD, allowing for vastly reduced time and costs in the research and design sector, [15].Modern optimisation methods tend to use surrogate modelling to accurately find the best solution. Surrogate modelling is a powerful tool involving creating a function to approximate the relationship between the inputs (variables) to the outputs (results). These functions are typically built from the ground up, using experimental data with different input variables. These functions can then be solved to find the maximum or minimum point, or for multi-objective scenarios, the best compromise. [16]

The two most popular surrogate modelling methods are Response Surface Methodology (RSM) and Kriging. RSM uses a polynomial function to approximate the correlation and is relatively straightforward to use. As such, it is a very popular method for optimisation problems in a wide variety of areas. [17]

Kriging, also known as Design and Analysis of Computer Experiments (DACE), is a statistical method for predicting the behaviour of a function with unknown inputs, introduced by Santner, Williams and Notz in 1989, [18] It is another form of surrogate modelling but differs from RSM as it does not rely solely on a polynomial model. For some complex problems, this model can not fully approximate the relationship between variables and results. Kriging uses a global polynomial model, with a covariance matrix handling local deviations. This allows for more complex response surface plots with the ability to show smaller peaks and valleys that RSM may not capture. This increased accuracy and detail in local areas gives Kriging functions more versatility, allowing them to conform to more complex models, [19]. Kriging has not seen the widespread use in engineering applications that RSM has due to its complex nature and inherent difficulty to use. Fortunately, there are now tools to assist with analysis, such as the ooDACE toolbox for MATLAB, [20]. This paper will use Kriging with the ooDACE toolbox for MATLAB.

Careful consideration must be taken when planning the experimenting process in an optimisation problem. It is important to design the experiments so that the full range of each variable is explored, and good analysis can be undertaken. This will allow solid, accurate conclusions to be drawn from the experimenting process. This paper will use Latin Hypercube sampling (LHS). It is a semi-random technique which aims for a good distribution of values across the range of each of the factors. This ensures each variable is properly explored and defined, leading to a better understanding of the optimisation problem. This technique is particularly useful for variables with a wider range, such as the current study, where the distance between notches could be varied from 20mm to 40mm, for example. [21]

3. Results
3.1 CFD Model Validation

The results are validated against experimental results from the test rig. The test rig results can vary from atmospheric conditions on the day of the test, so the mean of 6 sets of results is used for the comparison. The results for friction factor and Colburn factor are shown in Figure 2 & Figure 3. Error bars are added to show the standard error at each Reynolds number point. The simulated data is close to the mean values of the test rig data and well within the standard error at each point. The model is deemed to satisfy the conditions of validation and can be used for further research. N.B. The project industrial sponsor has requested the detailed performance data of their element design be omitted.
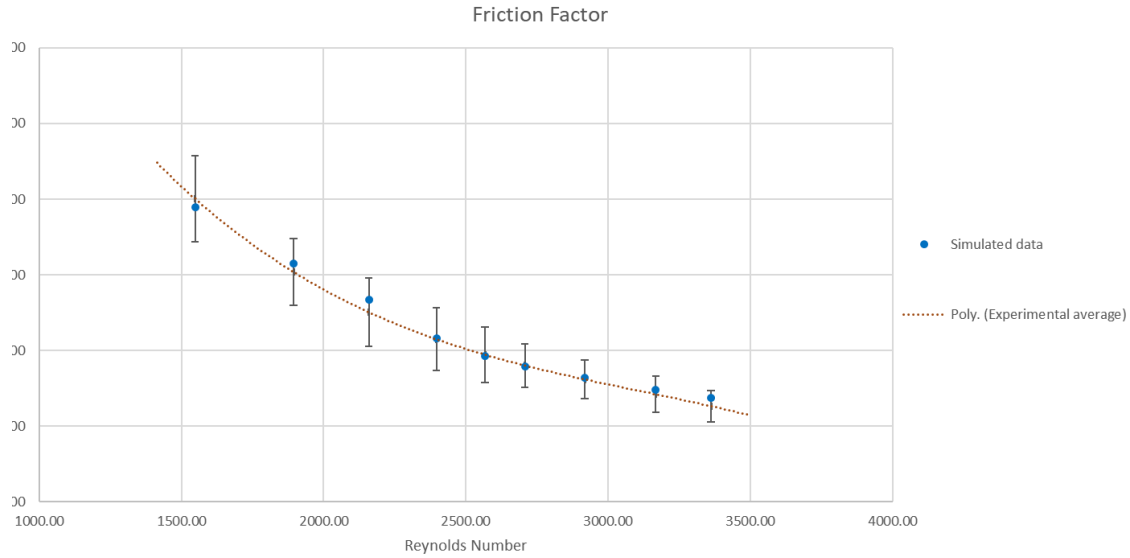
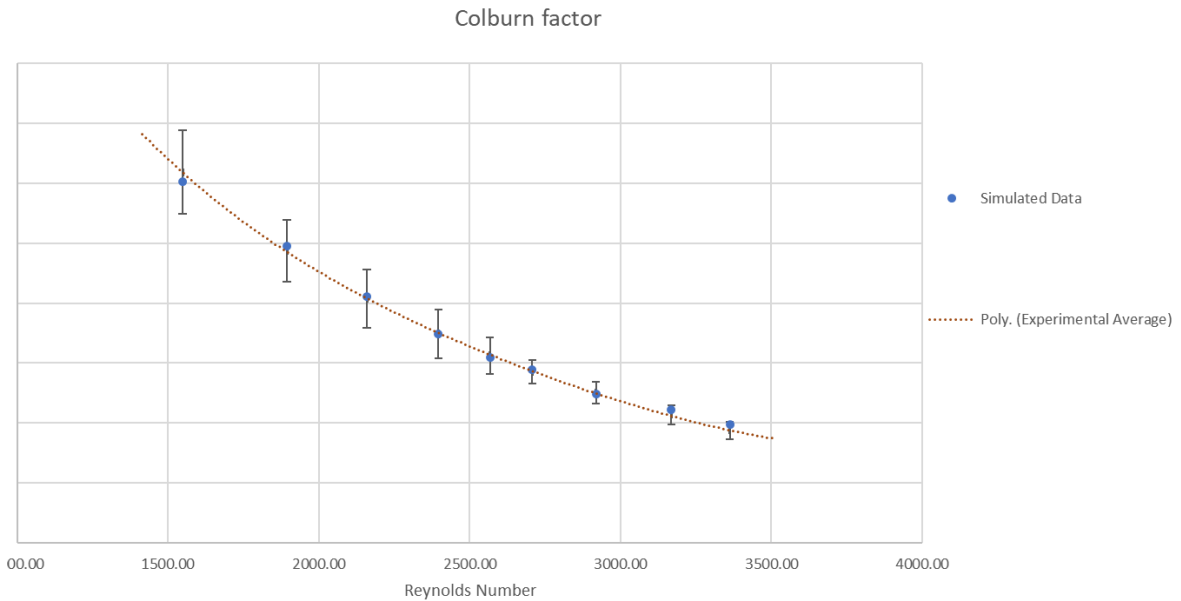Figure 2.Friction factor simulated data and experimental data comparison

Figure 3. Colburn factor simulated data and experimental data comparison

3.2 Optimisation

The results from the optimisation code are presented in Figure 4 and Figure 5 as 3D plots, with the variables on the horizontal X and Y axes and the results on the vertical Z axis. There are some clear areas of interest upon visual inspection: the valley around pitch 37mm in the friction factor plot, with a corresponding high area in the Colburn factor plot, and the trough in the pitch 30mm/radius 4mm corner in the friction factor plot, with the corresponding peak in the Colburn factor plot. The low friction factor and high Colburn factor areas are undoubtedly the best performing areas. Using the MATLAB pareto-search function, the optimal points in these areas were found (Table 2). As predicted, the best performing points are located within the pitch 37mm valley and the pitch 30mm/radius 4mm corner. "Optimal Result 1" has a reasonable improvement in both the friction factor and colburn factor, and "Optimal Result 2" has a much higher improvement in friction factor with a lesser improvement in Colburn factor. "Optimal Result 1" is the approprioate choice for this study. N.B. The project industrial sponsor has requested the detailed performance data of their element design be omitted.

Table 2. Optimisation results

	Pitch (mm)	Radius (mm)	FF % decrease	CF % increase
Original Flat Notched Crossed	Confidential	Confidential	0.0	0.0
Best FF	31.6	4.00	10.7	1.6
Best CF	37.9	2.43	1.9	2.9
Optimal Result 1	36.9	2.67	7.3	2.3
Optimal Result 2	31.2	4.00	10.2	1.8
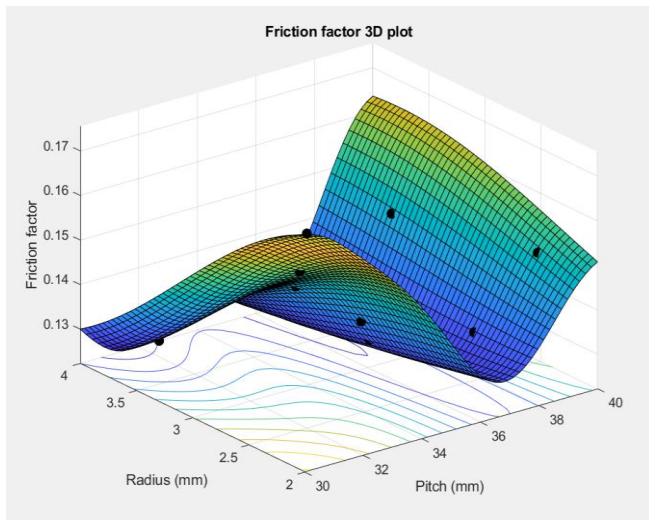
Figure 4. Friction Factor 3D optimisation plot
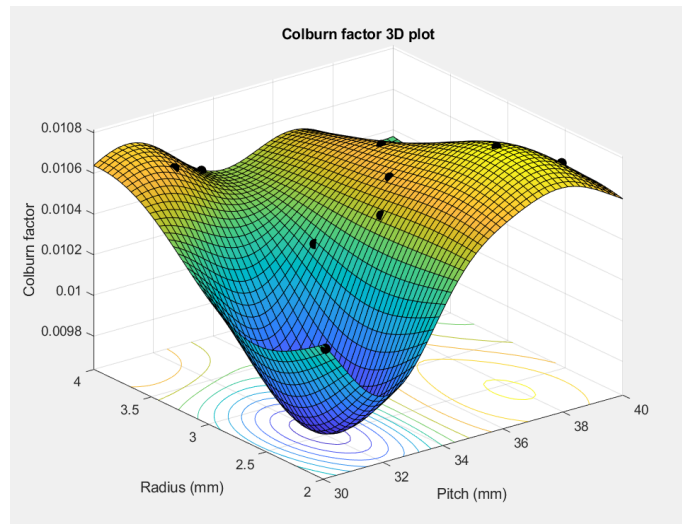
Figure 5. Colburn factor 3D optimisation plot

A model was created from the dimension listed in "Optimal Result 1" and a CFD simulation was run on it. The results are shown in Table 3. The friction factor result is 1% higher than the predicted result. This particular error can be attributed to the sensitivity of the friction factor to minute differences in the design. This is believed to be due to rounding in the pitch and radius variables. This issue is unavoidable, as the tolerances for manufacture for the element plates will not realistically achieve accuracy for measurements smaller than 0.1mm.

Table 3. Predicted results vs simulated results

	Friction Factor	Colburn Factor
Predicted	0.1270	0.01075
Simulated	0.128317621	0.01076
% Difference	1.04	0.09

The local heat transfer coefficient over the bottom Flat Notched Crossed plate is shown in Figure 6, along with the velocity profile in the flow direction at 3 planes across the plate. The optimised plate design is shown for comparison, and the areas where heat transfer is augmented are clear. The lighter coloured areas on the flat area of the plate correspond to higher local heat transfer rates from vortices created by the crossflow of the opposing notch angles of the two plates. This appears to show that the pitch and radius dimensions play a large part in allowing these vortices to fully develop, improving the overall turbulent mixing through the heat exchanger. These vortex structures can be clearly seen on the

velocity flow planes. It is also apparent that some parts of the element have significantly less "contact" with the flow, showing there is still room for further heat transfer augmentation.
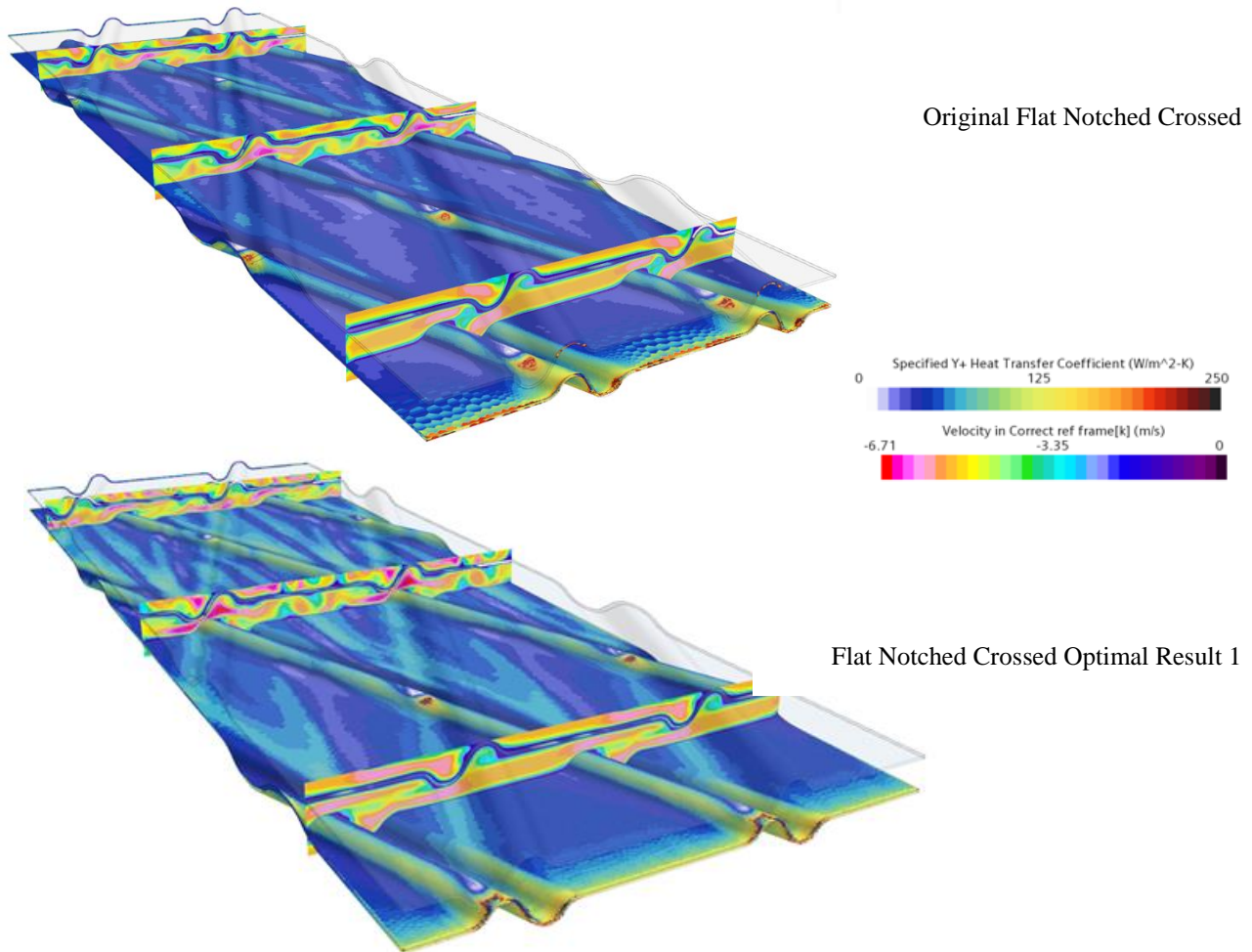

Figure 6. Local heat transfer and velocity flow planes over bottom Flat Notched Crossed plate

The stronger vortices can be seen clearly when comparing the velocity flow planes side by side (Figure 7). In the "middle" plane for the optimised results, there are 2 clear vortices in the flat areas in between the two plates, with several other less obvious vortices in other areas. The vortices are remarkably stronger and more visually obvious in the optimised model. This leads to the conclusion that the strength and control of these secondary flow structures is key to the increased performance of the plate design.
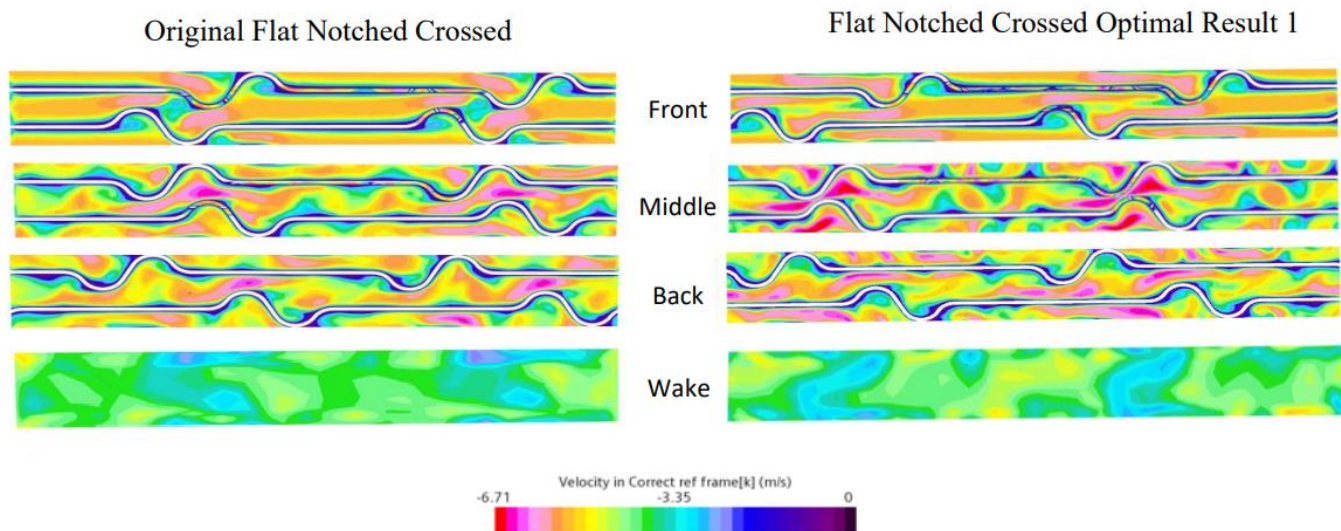
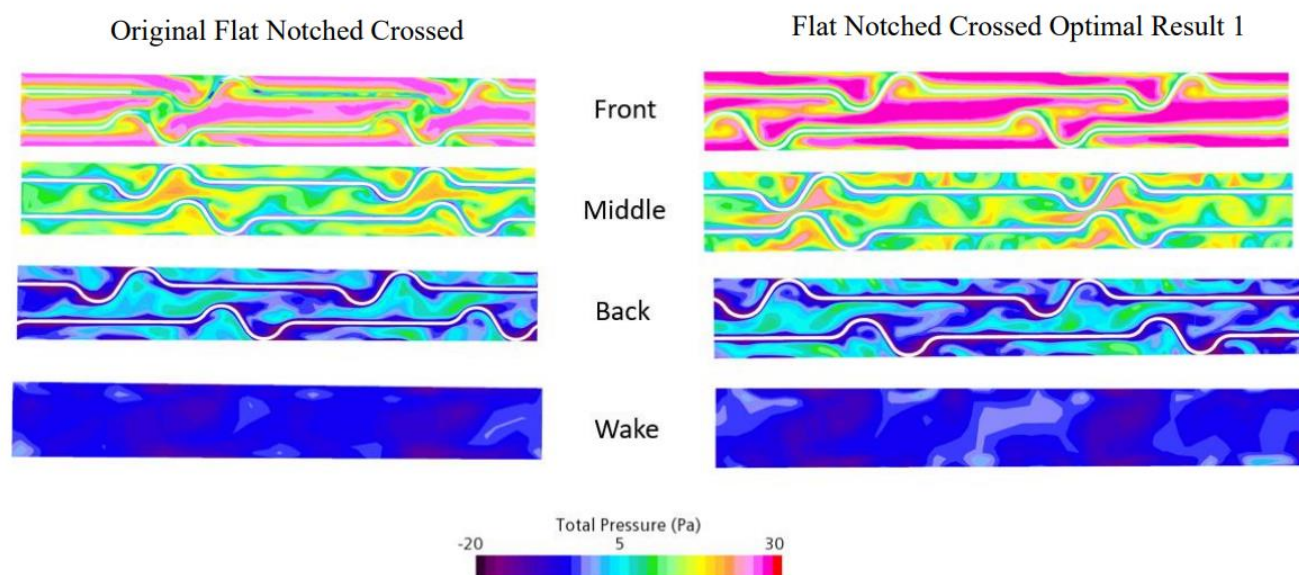Figure 7. Velocity flow plane view in Flat Notched Crossed plate

Figure 8. Pressure flow plane view in Flat Notched Crossed plate

From the pressure plane comparisons (Figure 8), the same effect can be seen. There are strong secondary flows present throughtout the heat exchanger, causing significantly increased turbulent mixing. This opens the door for further research into this area.

4. Conclusions

The Flat Notched Crossed plate has been successfully modelled and validated, and optimisation showed that a simple change in dimensions can completely change the flow characteristics of a rotary heater element plate. The conclusions that can be drawn are:

1. The optimised Flat Notched Crossed design has improved heat transfer while reducing the pressure drop. Depending on the use case, further improvement could be made in one of these characteristics, to the detriment of the other.

2. The main driver of heat transfer augmentation is turbulence and turbulent mixing. Inducing further turbulence with vortex generator style flow devices could be very beneficial to the performance of rotary heater elements.

3. Some parts of the elements contribute little to the heat transfer, so further performance gains could be avhieved by finding some way to benefit from these areas.

3. Controlling the secondary flow structures will result in further performance improvements. This could be in the form of guiding the vortices towards certain areas, or helping them develop further.

These conclusions are drawn from a simple dimension optimisation scheme, and could benefit from further work. Further work will include detailed analysis of secondary flow structures, vortex generation flow devices, and investiagtion into flow behaviours that augment heat transfer.

Acknowledgements

References

[1] L. Wang, Y. He, C. Tang, Y. Wang, and D. Che, 'A novel design of rotary regenerative condensing heat exchanger for the dehydration from high humidity flue gas', *Int J Heat Mass Transf*, vol. 131, pp. 517–526, Mar. 2019, doi: 10.1016/J.IJHEATMASSTRANSFER.2018.11.080.

[2] I. Warren, 'Ljungstrom heat exchangers for waste heat recovery', *J. Heat Recovery Syst.; (United Kingdom)*, vol. 2:3, no. 3, pp. 257–271, 1982, doi: 10.1016/0198-7593(82)90019-4.

[3] 'Analysis of Performance of Ljungstrom Air Preheater Elements', doi: 10.14741/ijcet/spl.2.2014.94.

[4] W. W. Focke and P. G. Knibbe, 'Flow visualization in parallel-plate ducts with corrugated walls', *J Fluid Mech*, vol. 165, 1986, doi: 10.1017/S0022112086003002.

[5] M. Ciofalo, I. di Piazza, and J. A. Stasiek, 'Investigation of flow and heat transfer in corrugated-undulated plate heat exchangers', *Heat and Mass Transfer/Waerme- und Stoffuebertragung*, vol. 36, no. 5, pp. 449–462, Sep. 2000, doi: 10.1007/S002310000106.

[6] Y. M. Lee, H. Chung, S. H. Kim, H. S. Bae, and H. H. Cho, 'Optimization of the Heating Element in a Gas-Gas Heater Using an Integrated Analysis Model', *Energies 2017, Vol. 10, Page 1932*, vol. 10, no. 12, p. 1932, Nov. 2017, doi: 10.3390/EN10121932.

[7] J. A. Stasiek, 'Experimental studies of heat transfer and fluid flow across corrugated-undulated heat exchanger surfaces', *Int J Heat Mass Transf*, vol. 41, no. 6–7, pp. 899–914, 1998, doi: 10.1016/S0017-9310(97)00168-3.

[8] Z. Zou, F. Shao, Y. Li, W. Zhang, and A. Berglund, 'Dominant flow structure in the squealer tip gap and its impact on turbine aerodynamic performance', *Energy*, vol. 138, pp. 167–184, Nov. 2017, doi: 10.1016/J.ENERGY.2017.07.047.

[9] R. Bensow, C. Fureby, M. Liefvendahl, and T. Persson, 'A Comparative Study of RANS, DES and LES', Apr. 2006.

[10] '[PDF] Comparison of RANS and LES Turbulence Models against Constant Volume Diesel Experiments | Semantic Scholar'. https://www.semanticscholar.org/paper/Comparison-of-RANS-and-LES-Turbulence-Models-Volume-Som-Senecal/42a68199923a49eafdfabf91b4821eb3dfe01a12 (accessed Apr. 24, 2022).

[11] R. B. Bird, W. E. Stewart, and E. N. Lightfoot, 'Transport Phenomena , 2nd Edition', *Transport Phenomena*, pp. 422–453, 2002.

[12] U. Besson, 'The History of the Cooling Law: When the Search for Simplicity can be an Obstacle', doi: 10.1007/s11191-010-9324-1.

[13] F. P. Incropera, D. P. DeWitt, T. L. Bergman, and A. S. Lavine, *Fundamentals of Heat and Mass Transfer-Incropera*, 7th ed. 2011. Accessed: Nov. 24, 2020. [Online]. Available: https://books.google.com/books/about/Fundamentals_of_Heat_and_Mass_Transfer.html?id=vvyIoXEywMoC

[14] J. K. Lunowa, 'Darcy Friction Factor Formulae in Turbulent Pipe Flow', 2011, Accessed: Apr. 24, 2022. [Online]. Available: http://www.kolumbus.fi/jukka.kiijarvi/clunowa/clunowa.html

[15] J. W. Bandler *et al.*, 'Space mapping: The state of the art', *IEEE Trans Microw Theory Tech*, vol. 52, no. 1 II, pp. 337–361, Jan. 2004, doi: 10.1109/TMTT.2003.820904.

[16] R. H. Myers, 'Response Surface Methodology—Current Status and Future Directions', *https://doi.org/10.1080/00224065.1999.11979891*, vol. 31, no. 1, pp. 30–44, 2018, doi: 10.1080/00224065.1999.11979891.

[17] G. E. P. Box and K. B. Wilson, 'On the Experimental Attainment of Optimum Conditions', *Journal of the Royal Statistical Society. Series B (Methodological)*, vol. 13, no. 1, pp. 1–45, 1951, Accessed: Apr. 25, 2022. [Online]. Available: https://www-jstor-org.ezproxy.lib.gla.ac.uk/stable/2983966?pq-origsite=summon&seq=1

[18] J. Sacks, W. J. Welch, T. J. Mitchell, and H. P. Wynn, 'Design and Analysis of Computer Experiments', *https://doi.org/10.1214/ss/1177012413*, vol. 4, no. 4, pp. 409–423, Nov. 1989, doi: 10.1214/SS/1177012413.

[19] T. W. Simpson, T. M. Mauery, J. J. Korte, and F. Mistree, 'Comparison of response surface and kriging models for multidisciplinary design optimization', *7th AIAA/USAF/NASA/ISSMO Symposium on Multidisciplinary Analysis and Optimization*, pp. 381–391, 1998, doi: 10.2514/6.1998-4755.

[20] '(PDF) ooDACE Toolbox: A Flexible Object-Oriented Kriging Implementation'. https://www.researchgate.net/publication/288622572_ooDACE_Toolbox_A_Flexible_Object-Oriented_Kriging_Implementation (accessed Jan. 04, 2023).

[21] K.-T. Fang, R. Li, and A. Sudjianto, 'Design and Modeling for Computer Experiments (Chapman & Hall/CRC Computer Science & Data Analysis)', 2005, Accessed: Apr. 25, 2022. [Online]. Available: http://www.amazon.com/exec/obidos/redirect?tag=citeulike07-20&path=ASIN/1584885467